J Electroceram (2010) 24:237–244
DOI 10.1007/s10832-009-9564-0

# Effect of mechanical loading on the tuning of acoustic resonances in $Ba_xSr_{1-x}TiO_3$ thin films

**A. Noeth · T. Yamada · A. K. Tagantsev · N. Setter**

Received: 28 August 2008 / Accepted: 14 January 2009 / Published online: 28 January 2009


**Abstract** The effect of mechanical loading on the tuning performance of a tunable Thin Film Bulk Acoustic Wave Resonator (TFBAR) based on a $Ba_{0.3}Sr_{0.7}TiO_3$ (BST) thin film has been investigated experimentally and theoretically. A membrane-type TFBAR was fabricated by means of micromachining. The mechanical load on the device was increased stepwise by evaporating $SiO_2$ on the backside of the membrane. The device was electrically characterized after each evaporation step and the results were compared to those obtained from modeling. The device with the smallest mechanical load exhibited a tuning of −2.4% and −0.6% for the resonance and antiresonance frequencies at a dc electric field of 615 kV/cm, respectively. With increasing mechanical load a decrease in the tuning performance was observed. This decrease was rather weak if the thickness of the mechanical load was smaller or comparable to the thickness of the active BST film. If the thickness of the mechanical load was larger than the thickness of the active BST layer, a significant reduction in the tuning performance was observed. The weaker tuning of the antiresonance frequency was due to a reduced tuning of the sound velocity of the BST layer with increasing dc bias. The resonance frequency showed a reduced tuning due to a decrease in the effective electromechanical coupling factor of the device with increasing mechanical load. With the help of the modeling we could de-embed the intrinsic tuning performance of a single, non-loaded BST thin film. We show that the tuning performance of the device with the smallest mechanical load we fabricated is close to the intrinsic tuning characteristics of the BST layer.

**Keywords** BST · Tunable · BAW · FBAR

A. Noeth (✉) · A. K. Tagantsev · N. Setter
Ceramics Laboratory, Swiss Federal Institute of Technology (EPFL), 1015 Lausanne, Switzerland
e-mail: andreas.noeth@epfl.ch

T. Yamada
Department of Innovative and Engineered Materials, Tokyo Institute of Technology, 4259 Nagatsuta-cho, Midori-ku, Yokohama 226-8502, Japan

## 1 Introduction

Thin films of $Ba_xSr_{1-x}TiO_3$ (BST) in the paraelectric centrosymmetric phase are of interest for high frequency tunable devices like phase shifters [1, 2], tunable filters [3, 4], voltage controlled oscillators [5, 6], etc. The interest is due to the dc electric field dependent permittivity of BST which is reduced with increasing dc bias. The applied dc electric field also leads to a displacement of ions in the material unit cell, which results in a break of the central symmetry of its crystal structure so that the material behaves like a piezoelectric. Based on this dc bias induced piezoelectricity, Thin Film Bulk Acoustic Wave Resonators (TFBARs) with BST thin films have been recently developed [7–9] where it was found that both resonance and antiresonance frequency are dc bias dependent [10]. For BST thin films in the paraelectric phase it was observed that the antiresonance frequency shows a weaker dc bias dependence than the resonance frequency. Both frequencies shift to lower frequencies with increasing dc bias. In a theoretical treatment of the electrical tuning of dc bias induced acoustic resonances in BST

thin films, it was found that the tuning of resonance and antiresonance frequencies are a function of the dc bias dependent intrinsic electromechanical coupling factor $k^2_{BST}$ of the BST layer [11]. Moreover, it was shown that the intrinsic electromechanical coupling factor $k^2_{BST}$ and the relative tunability $n_r$ of the material permittivity are identical functions of the dc electric field. The higher the relative dielectric tunability of the BST thin film for a given device, the higher the dc bias induced intrinsic electromechanical coupling factor $k^2_{BST}$ of the BST layer and the higher the tuning of the resonance and antiresonance frequencies.

Characterizing a TFBAR one uses the effective electromechanical coupling factor $k^2_{eff} = 4/\pi^2(\omega_{ares} - \omega_{res})/\omega_{ares}$ (where $\omega_{res}$ and $\omega_{ares}$ are the resonance and antiresonance frequencies of the device, respectively) which may substantially differ from the $k^2_{BST}$ of the used piezoelectric material [12]. The effective electromechanical coupling factor depends not only on materials parameters of the piezoelectric thin film but also on the device design. Concerning the device design, it is known that a mechanical load can reduce its $k^2_{eff}$. The mechanical load comprises all non-piezoelectric layers (e.g. electrodes, support layers, etc) building the TFBAR. Nakumura et al. [13] modeled the dependence of the $k^2_{eff}$ on the ratio of the thicknesses of the piezoelectric layer and the TFBAR device. For the fundamental mode resonance ($\lambda/2$) it was found that $k^2_{eff}$ decreases with increasing mechanical load. Ivira et al. [14] found that $k^2_{eff}$ of an Aluminium Nitride (AlN) TFBAR with a fixed thickness of molybdenum electrodes decreases with increasing thickness of a $SiO_2$ layer attached to the device.

In this paper we study experimentally and theoretically the effect of mechanical load on the tuning of the dc bias induced acoustic resonances of a BST based membrane-type TFBAR. The mechanical load of the device was increased stepwise by evaporating $SiO_2$ through the hole on the backside of the silicon wafer. After each evaporation step the device was electrically characterized. In addition to the experiments the device with different mechanical loads was modeled with the electrical impedance formula for composite resonators developed by Lakin [15]. With the help of the modeling we were able to extract the intrinsic electromechanical parameters of the BST thin film. Our experimental and theoretical investigations show that the device with the minimum mechanical load we investigated shows only a slightly reduced tuning in comparison to the intrinsic tuning properties of the BST layer. The impact of the size and asymmetric distribution of the mechanical load on the tuning of TFBAR devices is discussed.

## 2 Experimental

A BST based membrane type TFBAR has been fabricated by means of microfabrication. The device was fabricated starting from a high resistive silicon wafer ($\rho > 10$ k$\Omega$ cm). The wafer surfaces were oxidized by dry oxidation resulting in 100 nm thick $SiO_2$ layers. A 100 nm thick Pt bottom electrode has been deposited on the topside of the wafer using $TiO_2$/Ti adhesion layers. The deposited bottom electrode was structured by dry etching (ICP) resulting in a square-shaped electrode of 270 $\mu$m edge length. A BST (x= 0.3) thin film was deposited on the wafer by means of pulsed laser deposition (PLD) with a KrF excimer laser ($\lambda = 248$ nm). The laser energy and the repetition rate were 220 mJ and 5 Hz, respectively. The deposition temperature and oxygen pressure were 600 °C and $5\times10^{-4}$ Torr. The film thickness was controlled to be 650 nm. The BST film exhibited a (001)/(111) preferred orientation as confirmed by x-ray diffraction analysis. After film deposition, the samples were annealed in air at 500 °C for 1h. A 300 nm thick Al top electrode with Ti adhesion layer was evaporated and patterned by lift-off process. In a final processing step, the silicon was locally etched from the backside of the wafer using the Bosch process. This process step liberated square-shaped membranes of 350 $\mu$m edge length. The Pt bottom electrode was centered on the membrane. A schematic viewgraph of the BST based TFBAR is shown in Fig. 1(a). The thicknesses of the different layers are: Al(300 nm), BST(650 nm), Pt(100 nm) and $SiO_2$(100 nm). The device was contacted using Cascade Microtech Ground - Signal - Ground (G-S-G) probes. The ground signal was capacitively coupled to the floating Pt bottom electrode. The high frequency electrical characterization of the device was performed with an HP network analyzer 8722D measuring the reflection coefficient $S_{11}$ at room temperature. The system was calibrated by the SOL (short-open-load) method using a Cascade calibration substrate. The resonance and antiresonance frequencies were determined from the maximum of the real part of the admittance and the impedance, respectively. The mechanical load on the device was increased by evaporating $SiO_2$ layers through the micromachined hole on the backside of the wafer. The $SiO_2$ thickness was increased in 100 nm steps up to a maximum thickness of 700 nm (Fig. 1(b)). A calibration was performed to ensure that exactly 100 nm $SiO_2$ are deposited on the backside of the membrane structure. After each evaporation step, the device was electrically characterized. All experiments were performed on one single device.

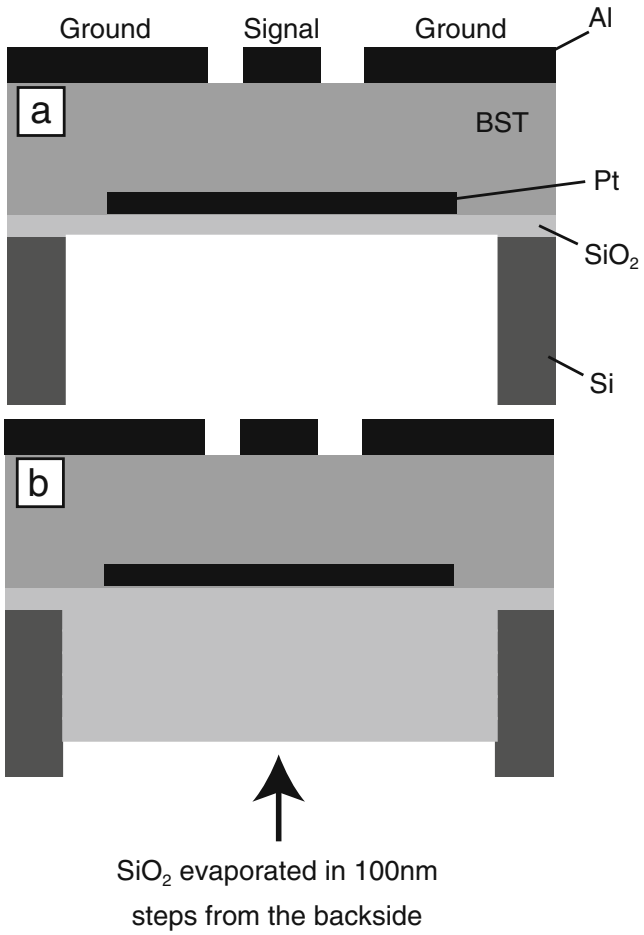


**Fig. 1** Schematic cross section of the fabricated device. The layer thicknesses of the TFBAR in (**a**) are: Al(300 nm), BST(650 nm), Pt(100 nm), and $SiO_2$(100 nm). The thickness of $SiO_2$ was increased in 100 nm steps by evaporating $SiO_2$ through the micromachined hole on the backside of the wafer as shown in (**b**). The maximum thickness of $SiO_2$ was 700 nm

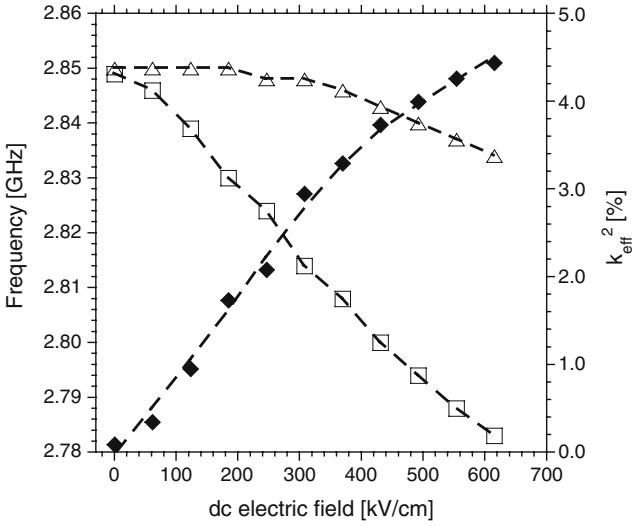


**Fig. 2** Dependence of the resonance (*open squares*) and antiresonance frequency (*open triangles*) and the effective electromechanical coupling factor $k^2_{eff}(exp)$ (*filled diamonds*) on the dc electric field for a BST TFBAR with a 100 nm thick $SiO_2$ layer as shown in Fig. 1(a). The resonance frequency at $E_{dc}$ extrapolated to 0 kV/cm is 2.850 GHz

## 3 Experimental results

Figure 2 shows the dependence of the resonance $\omega_{res}$ and the antiresonance frequency $\omega_{ares}$ as well as the experimentally determined effective electromechanical coupling factor $k^2_{eff}(exp)$ on the dc electric field for the BST TFBAR with a 100 nm thick $SiO_2$ layer. The experimentally measured effective electromechanical coupling factor $k^2_{eff}(exp)$ was calculated as:

$$k^2_{eff}\,(exp) = \frac{\pi^2}{4}\frac{\omega_{ares} - \omega_{res}}{\omega_{ares}} \tag{1}$$

The antiresonance frequency shifted down by 16 MHz for a maximum applied dc electric field of 615 kV/cm. The antiresonance frequency is dc bias dependent due to the dc bias dependence of the elastic constant $c^D$ at constant electric displacement $D$, which leads to a change of the sound velocity of the BST layer with dc bias [11]. The resonance frequency shows a larger shift of 66 MHz at the maximum dc electric field. The shift of the resonance frequency with increasing dc bias is due to the dc bias dependence of the effective electromechanical coupling factor $k^2_{eff}$ and the BST sound velocity. Here, the contribution of the dc bias dependence of $k^2_{eff}$ is stronger than the contribution stemming from the change in the sound velocity of the BST layer. For the maximum dc electric field of 615 kV/cm, the $k^2_{eff}(exp)$ increased up to 4.4%. The $k^2_{eff}(exp)$ was also determined by using a Butterworth-Van Dyke (BVD) equivalent circuit model which also resulted in a value of 4.4% at an applied dc electric field of 615 kV/cm.

Figure 3 shows the tuning of the resonance frequency and the relative tunability $n_r$ as functions of the dc electric field for the devices with $SiO_2$ layers which are 100 nm and 700 nm thick. The relative dielectric tunability $n_r$ is defined as:

$$n_r = \frac{\varepsilon\,(0) - \varepsilon\,(E_{\max})}{\varepsilon\,(0)} \tag{2}$$

where $\varepsilon(0)$ and $\varepsilon(E_{max})$ are the permittivity at zero and maximum dc electric field, respectively. Figure 3 shows that, as expected, the relative dielectric tunability of the material is not affected by the mechanical load. For the devices with the two different mechanical loads, it was

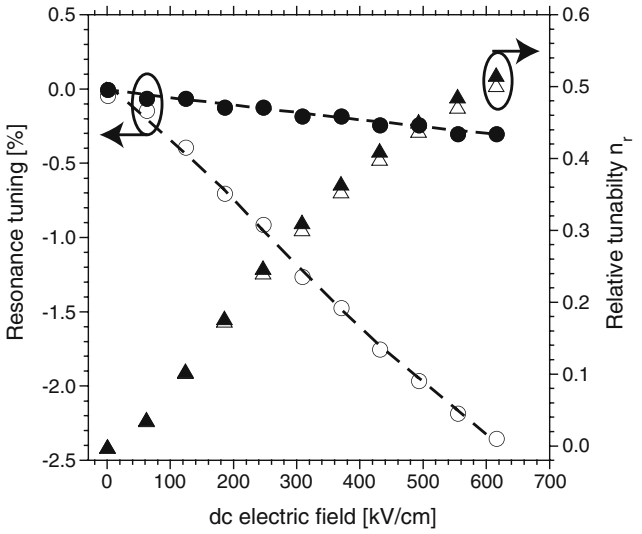


**Fig. 3** Dependence of the relative dielectric tunability $n_r$ and the tuning of the resonance frequency on the dc electric field for BST TFBARs with 100 and 700 nm thick $SiO_2$ layers. The relative tunabilities of the BST TFBAR with 100 nm $SiO_2$ (*open triangles*) and with 700 nm $SiO_2$ (*filled triangles*) are essentially the same at a given dc electric field. The tuning of the resonance frequency for the BST TFBAR with 100 nm $SiO_2$ (*open circles*) is stronger than the tuning of the resonance frequency of the BST TFBAR with 700 nm $SiO_2$ (*filled circles*)

≈50% at a maximum dc electric field of 615 kV/cm. The small difference in the relative tunability of the two measurements can be attributed to a change in temperature between the measurements or small calibration errors. In contrast to the relative tunability, the tuning of the resonance frequency is strongly reduced for the device with a 700 nm thick $SiO_2$ layer. From our theoretical analysis we expect that the magnitude of the intrinsic electromechanical coupling factor $k^2_{BST}$ in the BST layer should be the same for both devices since the layer shows the same relative tunability $n_r$ [11]. Thus, we conclude that the mechanical load leads to a strong reduction of $k^2_{eff}(exp)$ and also of the tuning of the acoustic resonances in the device.

## 4 Modeling

In order to better understand the influence of the mechanical load on the tuning of the acoustic resonances, modeling of the device with different mechanical loads was performed. The objectives of the modeling were to extract $k^2_{BST}$ of the BST layer and to estimate the impact of mechanical loading on tuning of the resonance and antiresonance frequencies of the whole system. The device with different mechanical loads was modeled by calculating its electrical impedance with the formula developed by Lakin for a composite resonator structure [15]:

$$Z = \frac{1}{i\omega C} \times \left[1 - k^2_{BST}\frac{\tan\phi}{\phi}\frac{(z_b + z_t)\cos^2\phi + i\sin 2\phi}{(z_b + z_t)\cos 2\phi + i\,(z_b\,z_t + 1)\sin 2\phi}\right] \quad (3)$$

where $\omega$ is the angular frequency, $C$ is the (clamped) capacitance, and $k^2_{BST}$ is the intrinsic electromechanical coupling factor of the BST layer. The phase $\phi$ across the BST layer is given by:

$$\phi_{BST} = \frac{kt_{BST}}{2} = \frac{\omega t_{BST}}{2v_{BST}} \quad (4)$$

where $k$, $t_{BST}$ and $v_{BST}$ are the propagation constant, the thickness, and the sound velocity of the BST layer at constant electric displacement $D$, respectively. The variables $z_b$ and $z_t$ are the normalized mechanical input impedances of the layers attached to the BST layer from the bottom and the top, respectively. These mechanical loading impedances are normalized with the mechanical impedance of the BST layer $Z_{BST}$:

$$z_b = \frac{Z_{in,b}}{Z_{BST}} \quad (5)$$

$$z_t = \frac{Z_{in,t}}{Z_{BST}} \quad (6)$$

The mechanical impedance of the BST layer is defined as:

$$Z_{BST} = \rho v_{BST} \quad (7)$$

where $\rho$ is the density of the BST layer. The mechanical input impedance $Z_{in}$ of each loading (non-piezoelectric) layer can be calculated using the transmission line equation as demonstrated in [15].

Mechanical losses were introduced as an imaginary part into the phase of the BST layer as proposed by Lanz [16]:

$$\phi_{loss} = \phi_{lossless}\left(1 - \frac{i}{2Q}\right) \quad (8)$$

where $\phi_{loss}$ and $\phi_{lossless}$ are the phase across the BST layer with and without acoustic losses, respectively. $Q$ corresponds to the mechanical Q-factor of the BST layer at antiresonance frequency. In our case a value of $Q = 100$ gave the best fits to the experimental data. We want to stress that we used $Q$ in Eq. 8 only as a fitting parameter. We considered only the mechanical losses neglecting the contribution of the electrical losses

to the total loss of the system. This explains the rather low values of $Q$ in comparison to bulk materials. A distinction between electrical and mechanical losses would need additional considerations. The mechanical losses of the layers attached to the BST layers were neglected, which can be justified by the fact that we managed to fit our data for different mechanical loads with the same values of $Q$. The acoustic properties of each layer used in the modeling are shown in Table 1. The sound velocity of the BST thin film at zero dc bias $v^0_{BST}$ can be estimated by solving the Christoffel equation [17]. The sound velocity of a quasi-longitudinal wave traveling in an arbitrary direction in cubic crystals varies between the sound velocity of the wave traveling in the (100) and the (110) direction of the crystal [17]. The sound velocity of a material can be calculated from its tensor of elastic constant $c_{ijkl}$ and its density $\rho$. The components of the tensor of the elastic constant $c_{ijkl}$ have been calculated for BST($x = 0.3$) in virtual crystal approximation, i.e. using linear interpolation between the values of parameters between the end members of the composition. With this method, the elastic constants $c_{11}$, $c_{12}$ and $c_{44}$ were calculated to be 283, 124 and 113 GPa, respectively. The density was calculated from the mass and the lattice parameters of the BST($x = 0.3$) unit cell which resulted in a value of 5413 kg/m$^3$. The sound velocity of a longitudinal wave traveling in the (100) and (110) can be calculated as:

$$v^0_{100} = \sqrt{\frac{c_{11}}{\rho}} \approx 7200\, m/s \tag{9}$$

$$v^0_{110} = \sqrt{\frac{c_{11} + c_{12} + c_{44}}{\rho}} \approx 10800\, m/s \tag{10}$$

For the modeling, a sound velocity at zero dc bias $v^0_{BST}$ of 6840 m/s for the BST layer gave the best fit to the experimental data. This value for the BST sound velocity is reasonable considering the (100) and (111) texture of the BST thin film and a certain variation of the BST film thickness across the sample. The sound velocity of the $SiO_2$ layer is ≈5950 m/s [18]. This value of the sound velocity gave a good fit to the data of the device shown in Fig. 1(a), where the 100 nm $SiO_2$ layer was deposited by dry oxidation. The evaporated $SiO_2$ (used for the device loading) seemed to show different acoustic properties than the $SiO_2$ layer deposited by dry oxidation. Therefore, we modeled the $SiO_2$ layers deposited by dry oxidation and evaporation as two different layers with different mechanical properties. For the evaporated $SiO_2$, a value of 4500 m/s for the sound velocity and $9.9\times10^6$ kg/m$^2$s for the mechanical impedance gave a better fit to our experimental data. A reduction in sound velocity might be due to a reduced elastic constant of our evaporated $SiO_2$ layers [19] and / or due to modified acoustic properties because of oxygen non-stoichiometry of the layer. The mechanical impedance of the evaporated $SiO_2$ layers was calculated with the sound velocity of 4500 m/s taking the theoretical density of the $SiO_2$ as 2201 kg/m$^3$. Using the aforementioned material parameters, we determined the field dependence of the intrinsic electromechanical coupling factor $k^2_{BST}$ by modeling the performance of the device containing only 100 nm $SiO_2$ (shown in Fig. 1(a)). The dc electric field dependence of the performance of the system was introduced in the modeling via a variation of the intrinsic electromechanical coupling factor $k^2_{BST}$ of the BST layer in Eq. 3. The resonance and antiresonance frequencies were determined as the maximum of the real part of the modeled admittance and impedance, respectively. From these values, the tuning of the resonance and antiresonance frequencies as well as the modeled effective electromechanical coupling factor $k^2_{eff}(mod)$ were calculated. The $\omega_{res}$ and $\omega_{ares}$ measured on the structure shown in Fig. 1(a) for different applied dc electric fields $E_{dc}$ were fit by changing $k^2_{BST}$. Thus, the dependence of $k^2_{BST}$ on $E_{dc}$ has been determined. At this point we were able to check a prediction of the theory of non-loaded tunable TFBARs, specifically the relation [11]:

$$A_t = \frac{k^2_{BST}}{n_r} \tag{11}$$

between $k^2_{BST}$ and the relative dielectric tunability $n_r$ of the BST layer. We have found this relation satisfied to within the experimental error. However the obtained value $A_t = 0.09$ is smaller than our estimates obtained from the thermodynamical parameters of BST (x= 0.3). Here, for thin films of (001) and (111) orientations, the values $A_t^{(001)} \approx 0.5$ and $A_t^{(111)} \approx 0.2$. were found [11]. For the moment we cannot comment this difference, which may be attributed to a poor

**Table 1** Material parameters used in the modeling of the BST TFBAR.

| Material | t [nm] | $Z_m \times 10^6$ [kg/m$^2$s] | v [m/s] |
|---|---|---|---|
| Al | 300 | 17.4 | 6380 |
| BST | 650 | 35.1 | 6840 |
| Pt | 100 | 57.6 | 2680 |
| $SiO_2$ (dry oxidation) | 100 | 12.6 | 5950 |
| $SiO_2$ (evaporation) | Variable | 9.9 | 4500 |

$Z_m$ corresponds to the mechanical impedance. The sound velocity and the mechanical impedance of BST correspond to the values at zero dc bias

knowledge of the thermodynamical parameters of the material.

Knowing the dependence of $k^2_{BST}$ on $E_{dc}$ or $n_r$ and using Eq. 3 we were able to model the tuning of resonance and antiresonance frequencies of the BST TFBAR with different mechanical loads and deembed the tuning of the non-loaded active layer.

Like mentioned above the shift of the antiresonance frequency is due to the dc bias dependence of the elastic constant $c^D$ of the BST layer at constant $D$. The sound velocity of the BST layer at constant $D$ is given by the relation [11]:

$$v_{BST} = \sqrt{\frac{c^D_{BST}}{\rho}} = v^0_{BST}\left(1 - k^2_{BST}\left(\gamma_t + \frac{\mu}{2}\right)\right) \tag{12}$$

where $\rho$ is the density of the BST layer and $v^0_{BST}$ is the sound velocity of the BST layer without dc bias and the parameters $\gamma_t$ and $\mu$ are defined as [11]:

$$\gamma_t \approx \frac{m}{8q^2\varepsilon} \tag{13}$$

$$\mu \approx \frac{\varepsilon^b}{\varepsilon} \tag{14}$$

where $q$, $m$, $\varepsilon$, $\varepsilon^b$ are the corresponding components of the tensor of linear electrostriction, nonlinear electrostriction, permittivity, and the background permittivity, respectively. The sum $\gamma_t + \mu/2$ is dc bias dependent due to the dc bias dependence of the permittivity of the BST thin film. In our modeling a value of ≈0.16 for the sum $\gamma_t + \mu/2$ for the maximum dc electric field gave the best fit to our experimental data.

## 5 Discussion

Figure 4 shows the experimental and modeled results for the resonance frequency of the BST TFBAR with different $SiO_2$ thicknesses at a dc bias extrapolated to the value $E_{dc} = 0$ kV/cm. The modeled results fit the experimental results very well. The small differences between the experimental and modeled values can be due to inaccurate determination of the thicknesses of the different layers of the device as well as inaccurate material data used in the modeling.

Figure 5 illustrates the experimental and modeled data of the tuning of the resonance and antiresonance

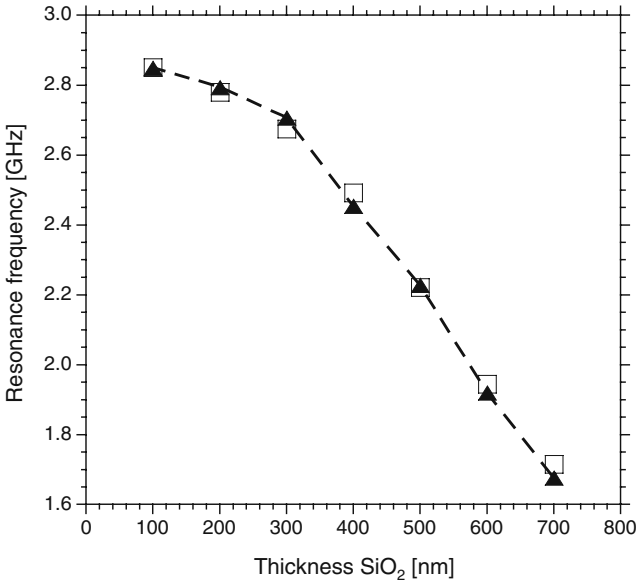


**Fig. 4** Modeled (*open squares*) and experimental (*filled triangles*) values of the resonance frequency at $E_{dc}$ extrapolated to 0 kV/cm for different thicknesses of the $SiO_2$ layer attached to the BST TFBAR

frequencies of the BST TFBAR with different $SiO_2$ thicknesses. The tuning of resonance $n_{res}$ and antiresonance frequency $n_{ares}$ is defined as:

$$n_{res} = \frac{\omega_{res}\left(E_{\max}\right) - \omega\left(0\right)}{\omega\left(0\right)} \tag{15}$$

$$n_{ares} = \frac{\omega_{ares}\left(E_{\max}\right) - \omega\left(0\right)}{\omega\left(0\right)} \tag{16}$$

where $\omega_{res}(E_{max})$, $\omega_{ares}(E_{max})$ and $\omega(0)$ are the resonance frequency at maximum dc bias, the antiresonance frequency at maximum dc bias, and the resonance frequency at $E_{dc}$ extrapolated to 0 kV/cm, respectively. Up to a thickness of 300 nm of $SiO_2$, $|n_{res}| \geq 2.0\%$ and $|n_{ares}| \geq 0.5\%$. For a $SiO_2$ thickness larger than 300 nm, $n_{res}$ and $n_{ares}$ are strongly reduced. We attribute this behavior with increasing mechanical load to two effects: First, the increase and asymmetric distribution of the mechanical load leads to a reduction in $k^2_{eff}$, which primarily reduces $n_{res}$. Second, the increase of the mechanical load leads to a reduced field induced change of the sound velocity in the TFBAR structure for a given dc electric field, which manifests itself in a reduction of $n_{ares}$.

From the modeling, $k^2_{BST}$ of the BST layer was determined to be 4.4% at a maximum dc electric field of 615 kV/cm. For a thickness of $SiO_2$ of up to 300 nm, $k^2_{eff}(exp) \geq 4\%$, which means that the effect of the

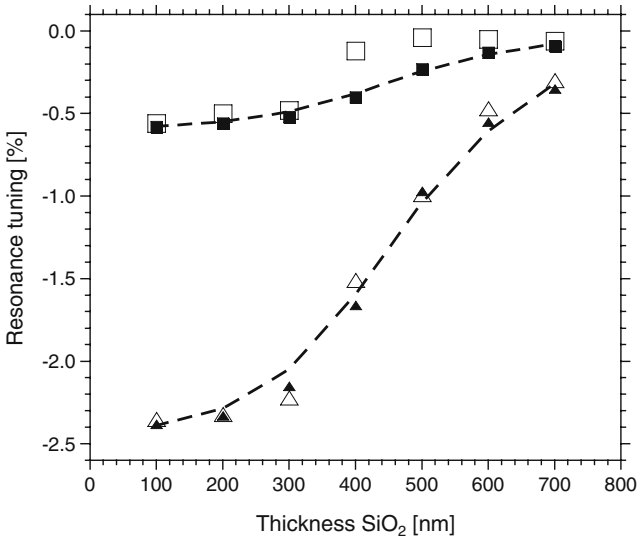


**Fig. 5** Modeled and experimental dependence of the tuning of resonance and antiresonance frequencies on the thickness of the $SiO_2$ layer. The experimental values for the tuning of the resonance and antiresonance frequencies are shown by (*open triangles*) and (*open squares*), respectively. The modeled values for the tuning of the resonance and antiresonance frequencies are shown by (*filled triangles*) and (*filled squares*), respectively

mechanical load on $k^2_{eff}(exp)$ is rather weak. We attribute this observation to a rather symmetrical distribution of the mechanical load via the following arguments. In this case, the maximum strain associated with the traveling acoustic wave of fundamental mode ($\lambda/2$) occurs in the BST layer. This results in a strong coupling in the BST layer, and therefore in a large $n_{res}$. A further increase of the $SiO_2$ load, leads to an asymmetric distribution of the mechanical load. In this case the point of maximum strain in the TFBAR structure is displaced and might not occur in the BST layer. In this case, the coupling in the BST layer is reduced which leads to a reduced $n_{res}$.

The reduction of $n_{ares}$ with increasing $SiO_2$ load is due to a reduced impact of the dc bias on the change of the sound velocity in the TFBAR structure. If we consider only the BST layer, the antiresonance frequency is given by:

$$\omega_{ares} = \frac{v_{BST}}{2t_{BST}} \tag{17}$$

The tuning of the antiresonance frequency is due to the dc bias dependence of the sound velocity of the BST thin film:

$$\frac{\Delta\omega_{ares}}{\omega_{ares}} = \frac{\Delta v_{BST}}{v^0_{BST}} \tag{18}$$

The layers loading the piezoactive BST layer do not show a dc bias dependence of the sound velocity. This means that with a mechanical load, one reduces the fraction of the traveling distance of the acoustic wave, where the sound velocity can be tuned. If a mechanical load is added to the BST layer, the antiresonance frequency of the system is:

$$\omega_{ares} = \frac{1}{2\left(\frac{t_{BST}}{v_{BST}} + \frac{t_{load}}{v_{load}}\right)} \tag{19}$$

where $t_{load}$ and $v_{load}$ correspond to the thickness and the sound velocity of the load. By calculating the derivative of Eq. 19, the tuning of the antiresonance frequency $\Delta\omega_{ares}/\omega_{ares}$ can found:

$$\frac{\Delta\omega_{ares}}{\omega_{ares}} = \frac{\Delta v_{BST}}{v^0_{BST}} \frac{\frac{t_{BST}}{v^0_{BST}}}{\frac{t_{BST}}{v^0_{BST}} + \frac{t_{load}}{v_{load}}} \tag{20}$$

Equation 20 shows that for a given $\Delta v_{BST}$, the tuning of the antiresonance frequency is reduced with increasing the mechanical load. This explains our experimental and modeled results where we observed that the tuning of the antiresonance frequency reduces gradually with increasing the mechanical load. For the maximum mechanical load we investigated, the tuning of the antiresonance frequency is smaller than 0.05%.

All in all, a qualitative difference in the impact of the progressive mechanical loading on the tuning of resonance and antiresonance frequencies is expected: the deterioration of the tuning of the later with loading should be rather gradual whereas, for the former, this effect should start slowly with a further acceleration.

The modeling enabled us to deembed the intrinsic electromechanical properties of the BST layer without any mechanical load meaning a BST layer without electrodes and $SiO_2$ layer attached to it.

Comparing these parameters of the BST layer with those of the device with the smallest mechanical load (the device shown in Fig. 1(a)), we found that $k^2_{BST}$ of the BST layer is equal, within our accuracy, to $k^2_{eff}(exp)$ of the device. But the non-loaded BST layer exhibits a slightly enhanced tuning of both resonance and antiresonance frequencies in comparison to the device. The $n_{res}$ and $n_{ares}$ of the single BST layer were determined to be −2.5% and −0.7%, respectively, whereas the device with the weakest mechanical load (electrodes +100 nm $SiO_2$) exhibited $n_{res}$ and $n_{ares}$ of −2.4% and −0.6%, respectively. This means that the mechanical load of the device shown in Fig. 1(a) does not significantly reduce the tuning characteristics of the device and that the intrinsic field dependent electromechanical properties of the BST layer are efficiently used. The less sensitivity

of $k^2_{eff}$ on the minimal load in comparison to $n_{res}$ and $n_{ares}$ can be readily rationalized in the lines of the above discussion of the two kinds of the loading effect. Small and identical reductions of $n_{res}$ and $n_{ares}$ are due to the reduction of the tunability of the sound velocity given by Eq. 12. The $k^2_{eff}$ is virtually not affected which agrees with the above remarks about the efficiency of the electromechanical coupling of the device.

## 6 Conclusions

We investigated experimentally and theoretically the effect of mechanical loading on the tuning of the resonance and antiresonance frequencies of BST-based TFBARs. The combination of experimental and theoretical work allowed us to extract the intrinsic tuning properties of a non-loaded BST layer. We found that the tuning of both resonance and antiresonance frequency is reduced by the mechanical load attached to the BST layer. The tuning of the antiresonance frequency is affected by the mechanical load via a reduction of the fraction of the traveling distance of the acoustic wave where the sound velocity is tuned. The tuning of the resonance frequency is affected by the mechanical load via a reduction of the effective electromechanical coupling in the device. It has been shown that though the mechanical loading reduces the acoustical tunability of a TFBAR, the impact of the load of a thickness comparable to that of the BST layer can be rather mild when it is distributed around the BST layer in a rather symmetric way. The tuning properties of the BST TFBAR with the smallest mechanical load (as shown in Fig. 1(a)) we investigated, exhibits tuning characteristics close to the properties of a single, free-standing BST layer.

**Acknowledgements** This work was supported by the Swiss National Foundation and the EU $6^{th}$ FP project - NANOSTAR. The author gratefully acknowledges the possibility to use the photolithography equipment of the Institute de Photonique et dElectronique Quantiques (IPEQ) at EPFL.

## References

1. B. Acikel, T.R. Taylor, P.J. Hansen J.S. Speck, R.A. York, IEEE Microw. Compon. Lett. **12**(7), 237 (2002)
2. E.G. Erker, A.S. Nagara, Y. Liu, P. Periaswamy, T.R. Taylor, J. Speck, R.A. York, IEEE Microw. Guided Wave **10**(1), 10 (2000)
3. G. Sanderson, A.H. Cardona, T.C. Watson, D. Chase, M. Roy, J.M. Paricka, R.A. York, IEEE/MTT-S International Microw. Symp. 2007, 679, Honolulu, 3–8 June 2007
4. J. Nath, D. Ghosh, J.P. Maria, A.I. Kingon, W. Fathelbab, P.D. Franzon, M.B Steer, IEEE Trans. Microwave Theor. Tech. **53**(9), 2707 (2005)
5. M. Norling, A. Vorobiev, H. Jacobsson, S. Gevorgian, IEEE Trans. Microwave Theor. Tech. **55**(2), 361 (2007)
6. A. Victor, J. Nath, D. Ghosh, B. Boyette, J.P. Maria, M.B. Steer, A.I. Kingon, G.T. Stauf, Proc. IEEE Radio Wirel. Conf. **91** (2004)
7. J. Berge, A. Vorobiev, W. Steichen, S. Gevorgian, IEEE Microw. Compon. Lett. **17**(9), 655 (2007)
8. A. Volatier, E. Defay, M. Aid, A. N'hari, P. Ancey, B. Dubus, Appl. Phys. Lett. **92**(3), 032906 (2008)
9. X. Zhu, J.D. Phillips, A. Mortazawi, IEEE/MTT-S International Microw. Symp. 2007, 671, Honolulu, 3–8 June 2007
10. A. Noeth, T. Yamada, V.O. Sherman, P. Muralt, A.K. Tagantsev, N. Setter, J. Appl. Phys. **102**(11), 114110 (2007)
11. A. Noeth, T. Yamada, A.K. Tagantsev, N. Setter, J. Appl. Phys. **104**(9), 094102 (2008)
12. R. Aigner, in *Proc. of Third International Symposium on Acoustic Wave Devices for Future Mobile Communication Systems,* 85 (2007)
13. K. Nakamura, H. Sasaki, H. Shimizu, Electron. Lett. **17**(14), 507 (1981)
14. B. Ivira, P. Benech, R. Fillit, F. Ndagijimana, P. Ancey, G. Parat, IEEE Trans. Ultrason. Ferroelectr. Freq. Control **55**(2), 421 (2008)
15. K.M. Lakin, G.R. Kline, K.T. McCarron, IEEE Trans. Microwave Theor. Tech. **41**(12), 2139 (1993)
16. R. Lanz, PhD thesis, EPFL, 2004
17. J.F. Rosenbaum, *Bulk Acoustic Wave Theory and Devices,* 462, (Artec House Inc., USA 1988)
18. A. Devos, R. Cote, G. Caruyer, A. Lefevre, Appl. Phys. Lett. **86**(21), 211903 (2005)
19. O. Zywitzki, H. Sahm, M. Krug, H. Morgner, M. Neumann, Surf. Coat. Technol. **133–134**, 555 (2000)